Combustion and Flame 211 (2020) 8–17

Contents lists available at ScienceDirect

Combustion and Flame

journal homepage: www.elsevier.com/locate/combustflame

Structures and propagation speeds of autoignition-assisted premixed *n*-heptane/air cool and warm flames at elevated temperatures and pressures

Tianhan Zhang*, Yiguang Ju

Department of Mechanical and Aerospace Engineering, Princeton University, Princeton, NJ 08544, USA

ARTICLE INFO

Article history:
Received 11 May 2019
Revised 28 June 2019
Accepted 16 September 2019

Keywords:
Cool flame
Warm flame
Flame speed
Ignition Damköhler number
Autoignition

ABSTRACT

The laminar flame speeds and structures of near-limit autoignition-assisted cool and warm *n*-heptane/air flames at different ignition Damköhler numbers which are the ratios between flow residence time and the ignition delay time, elevated temperatures and pressures are studied computationally and analytically over a broad range of equivalence ratios. The primary objective of this work is to understand the effects of the ignition Damköhler number, mixture temperature, equivalence ratio, and pressure on the dynamics and structures of cool and warm flame propagation near the flammability limit. Different transitions among near-limit cool, warm, and hot flames are examined. The results show that both cool and warm flame structures and propagation speeds change dramatically with the increase of the ignition Damköhler number. Moreover, the dependence of normalized cool and warm flame speeds on the ignition Damköhler number is affected by the equivalence ratio, pressure, and flame regimes. Furthermore, for equivalence ratios within the hot flame flammability limits, the results show that there exist two flame speeds, one for the hot flame and the other for the cool flame. It is shown that the cool flame speed has a non-monotonic dependence on the initial mixture temperature due to the negative temperature coefficient (NTC) effect. However, the warm flame speed has a much weaker NTC effect and the hot flame speed only increases monotonically with the increase of the initial temperature. The results also reveal that the lean cool flame speed can be much higher than the hot flame speed near the NTC region. Finally, a simple analytical model for predicting the flame speed of autoignition assisted flames is developed. The model implies that the reduced activation energy of autoignition strongly affects the flame speed dependence on the ignition Damköhler number. The present results significantly advanced the understanding of the near-limit low temperature flame dynamics.

1. Introduction

In advanced compression-ignition engines such as homogeneous charge compression-ignition (HCCI) engines [1], reactivity-controlled compression-ignition engine (RCCI) [2], and spark assisted HCCI engines [3,4], the low-temperature ignition (LTI), cool and warm flames [5–9], and autoignition assisted flames [10] play a critical role in affecting flame propagation, combustion heat release and the performance at fuel-lean and high compression ratio conditions.

Cool flames have been studied in various flame geometries including heated burners [11], stirred reactors [12], spherically propagating flames [13], counterflow flames [14–17], planar propagating flames [5,18], droplet combustion [19–21], rapid compression machines [22] and so on. A recent review of cool flame dynamics can be found in [23]. The studies have shown that there exist cool and warm flame below the hot flame flammability limit and that cool flame and hot flame can coexist for mixtures above the hot flame flammability limit [9]. Unfortunately, many of these studies are limited to low mixture initial temperatures or chemically frozen boundary conditions at which effects of the autoignition on flame propagation is not considered. However, in advanced engines, the mixtures are compressed to high temperature and pressure, and the autoignition timescale is comparable to the burning time of cool and hot flames themselves [23]. As a result, flame propagation at engine conditions may be significantly influenced by partial autoignition of the mixture. For example, at near stoichiometric conditions, knocking formation in gasoline engines is an outcome of autoignition induced deflagration to detonation transition [24,25].

* Corresponding author.
E-mail address: tianhanz@princeton.edu (T. Zhang).

https://doi.org/10.1016/j.combustflame.2019.09.019
0010-2180/

For an ultra-lean mixture, although knocking may not be a challenging issue, the reduced flame speeds and flame Damköhler number will make the low temperature ignition and cool flames become critical in engine combustion [9,26]. At spark assisted HCCI conditions of lean n-heptane/air mixtures, Ju et al. identified low temperature and high temperature autoignition wave propagation as well as the cool flame, the hot flame, and the double flame structures [4]. For hot flames, Martz et al. investigated the combustion regimes of ignition-assisted flames under different temperature conditions and revealed the acceleration effect of autoignition on hot flames [27,28]. Pan et al. further showed non-monotonic relation between premixed flame speed and the initial temperature due to the NTC effect [9]. Ansari and collaborators discussed the key parameters affecting the autoignition assisted hot flame burning rate using different fuels [29]. Recent shock tube experiments revealed there exists a non-monotonic flame speed dependence on mixture initial temperature [26]. However, the numerical modeling only showed that a monotonic flame speed dependence on temperature. The reason for the difference between experiment and modeling was not clearly explained.

More recently, Ju investigated the pressure, equivalence ratio and flame size effects on both cool and hot flame speed and the flammability limit diagram [6]. Faghih et al. and Zhang et al. investigated effect of confinement and the dynamics of the autoignition assisted flames [30,31]. Krisman et al. identified autoignition assisted flame regimes based on the response of the hot flame location to the inlet flow speed and demonstrated the acceleration effect from the low and high temperature chemistry, respectively [10]. Different flame regimes such as burner stabilized flames, ignition stabilized flames, and low temperature chemistry affected flames were predicted. However, it remains unclear as how the flame speeds of the cool flame and warm flame depend on the ignition Damköhler number and whether a cool flame can propagate faster than a hot flame above the lean flammability limit. In addition, cool flame exists in both fuel lean and fuel rich conditions. It is not clear how autoignition affects the propagation of lean and rich cool flames differently. Furthermore, it is also not clear with the increase of the mixture initial temperature how a cool flame transitions to a warm flame, a double flame, and a hot flame [17]. Answering these questions requires detailed investigation of near-limit cool, warm, and hot flames under engine-like autoignition conditions.

The goal of this study is to investigate the effects of the autoignition and the ignition Damköhler number on the flame structures, propagation speeds, and chemical kinetics of lean and rich premixed cool flames, warm flames, and hot flames at different temperatures and pressures at near-limit conditions. Firstly, the cool and warm flame speeds are simulated within a wide range of ignition Damköhler numbers. Then, effects of pressure, initial temperature, and equivalence ratio on autoignition assisted flame propagation are investigated at different ignition Damköhler numbers. Different types of transitions between near-limit cool flame, warm flame, and hot flame are identified. Finally, a simple theoretical analysis is conducted to analyze the dependence of autoignition assisted flame speeds on the ignition Damköhler numbers. Comparisons between analytical and simulation results are made.

2. Numerical models and methods

In the present study, *n*-heptane is chosen as the fuel because it has low-temperature reactivity and is a major component of the Primary Reference Fuel (PRF). A reduced *n*-heptane/air mechanism [32] with 170 species and 962 reactions is produced from a detailed mechanism [33] by a multi-generation path flux analysis (PFA) [34] method.

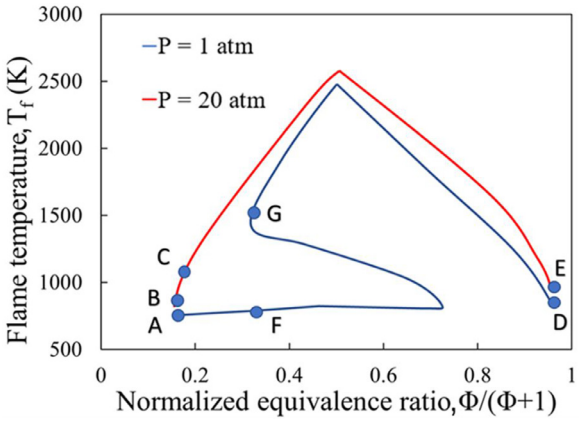

Fig. 1. The dependence of flame temperature on equivalence ratio of *n*-heptane/air mixture at 1 and 20 atm with initial temperature of 650 K. The dots mark the selected test cases.

In this study, both steady-state and unsteady freely propagating one-dimensional planar flames are used. For steady state flames, the results are cross-validated by using both methods. The detailed comparison between two methods can be found in the supplemental materials. PREMIX [35] is adopted as the steady-state solver in which the upstream domain length is adjusted to change the ignition Damköhler number. The distance between the leading flame front and the inlet boundary is varied from 1 mm to 5 cm depending on the ignition Damköhler number, ignition delay time and flame speed. The optical thin radiation model is adopted. The arc-length method [36] is used to accelerate finding the steady-state solutions.

For unsteady flame simulations, the ASURF+ [37,38] package is used. ASURF+ solves the compressible Navier–Stokes equations and the conservation equations of species and energy equations using the 3rd order weighted essentially non-oscillatory (WENO) scheme [39] and uses multi-level dynamically adaptive mesh refinement to resolve the flame front. In order to improve the computational efficiency, the correlated dynamic adaptive chemistry and transport (CO-DACT) method [40] and the hybrid multi-timescale (HMTS) method [41] are employed. To study the effect of the ignition Damköhler number on flame structure and dynamics, the length of preheating zone between the inlet boundary and the flame front, L_f, is pre-specified. The initial mixture temperature, T_0, equivalence ratio, ϕ and pressure, P, are given as the inlet boundary conditions. The ignition Damköhler number is then defined as,

$$Da_{ig} = \frac{\tau_f}{\tau_{ig}(T_0, P, \phi)} \tag{1}$$

where τ_{ig} is the autoignition delay time, for example, for cool and warm flames, τ_{ig} is the first stage ignition delay time, for hot flame, τ_{ig} is the second stage ignition delay time. $\tau_f \equiv L_f/S_L$ is the flow residence time from the boundary to the flame front, and S_L is the flame speed.

For initial conditions, a wide range of pressures, temperatures, and equivalence ratios are considered. Figure 1 shows the computed flammability diagram of *n*-heptane/air mixtures for $T_0 = 650\ K$, $\phi = 0.2 - 20$, $P = 1$ and 20 atm. Seven selected conditions, respectively for lean and rich cool flames, warm flame, and hot flame, are studied and marked on the flammability diagram in Fig. 1 [6]. The detailed simulation parameters for these seven cases are listed in Table 1. The flame speed dependence for ignition Damköhler number between 0.3 and 1.0 is examined for Case A, B, C and D. The relation between flame speed dependence on the mixture initial temperature at a given ignition Damköhler number is studied for Case A, B, C, D, E, F and G.

Table 1
Detailed parameters of selected test cases.

Position	Flame regime	Pressure (atm)	Equivalence ratio	Initial temperature (K)	Reference flame speed ($T = 650$ K) (cm/s)
A	Cool flame	1	0.2	650–1000	27.2
B	Cool flame	20	0.2	650–1000	5.6
C	Warm flame	20	0.25	650–1000	5.6
D	Cool flame	1	20	650–1000	22.4
E	Cool flame	20	20	650–900	7.7
F	Cool flame	1	0.5	650–900	28.6
G	Hot flame	1	0.5	650–900	77.7

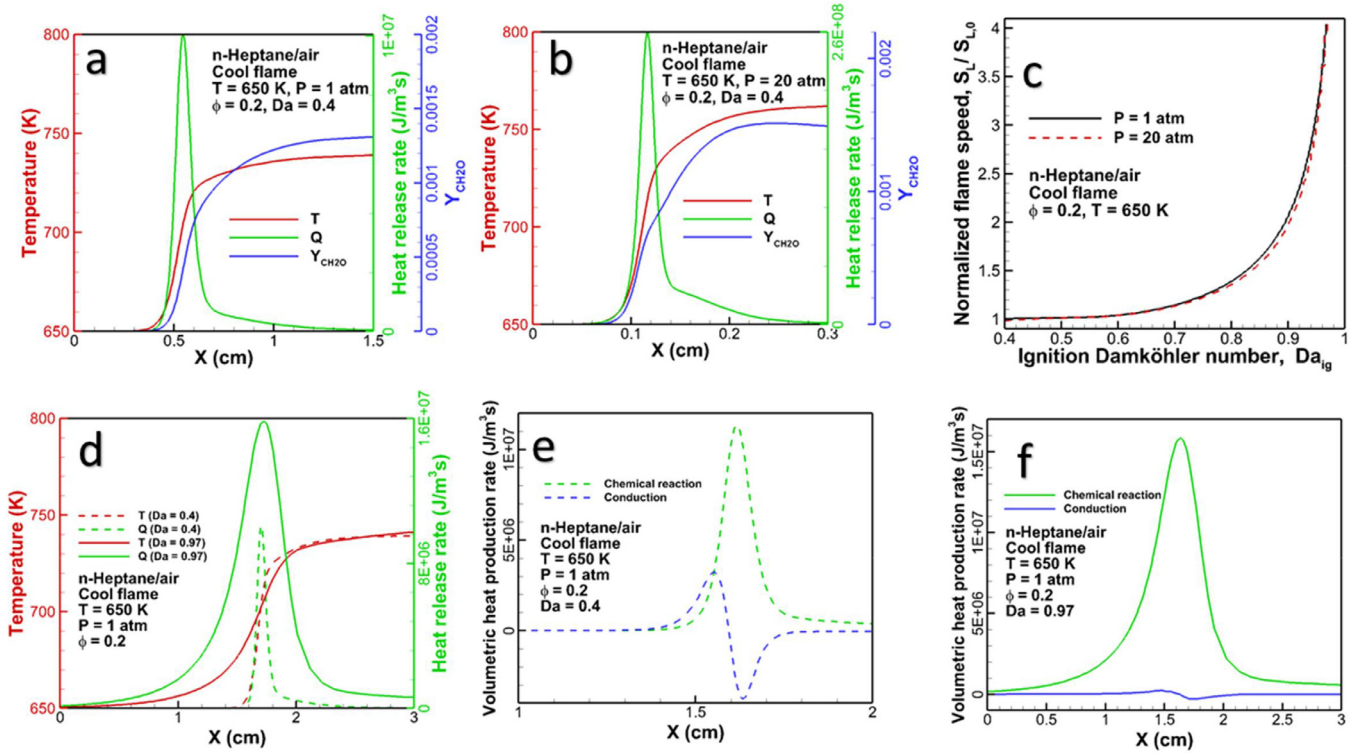

Fig. 2. a and b: the lean ($\phi = 0.2$) cool flame structures at $T_0 = 650$ K, $Da_{ig} = 0.4$, $P = 1$ (Case A) and 20 atm (Case B), respectively. (c) The relation between the normalized premixed cool flame speed and the ignition Damköhler number for lean cool flames at low and high pressures, $T_0 = 650$ K, $P = 1$ and 20 atm, $\phi = 0.2$. (d) The lean ($\phi = 0.2$) cool flame structures at $T_0 = 650$ K, $P = 1$ atm, $Da_{ig} = 0.4$ and 0.97, respectively. (e) and (f) Comparisons of the volumetric chemical heat release and heat conduction rates for cool flames at $T_0 = 650$ K, $P = 1$ atm, $\phi = 0.2$, $Da_{ig} = 0.4$ and 0.97, respectively.

3. Results and discussions

3.1. Effects of ignition Damköhler number on lean and rich cool flames at elevated pressures

Figure 2(a) and (b) shows the structures of lean ($\phi = 0.2$) cool flames at $T_0 = 650$ K, $P = 1$ (Case A) and 20 atm (Case B), respectively, at $Da_{ig} = 0.4$. The predicted cool flame speeds at 1 and 20 atm are $S_{L,Da_{ig}=0} = 27.2$ and 5.6 cm/s. Figure 2(a) shows that at $P = 1$ atm, the lean cool flame temperature rise is around 90 K and the effect of radiative heat loss on flame temperature is negligible. The cool flame reaction zone is very thin (~0.2 mm) and a large amount of formaldehyde is formed. At $P = 20$ atm, Fig. 2(b) shows that the cool flame temperature rises more than 110 K and the reaction zone thickness decreases to less than 0.04 mm. Moreover, CH_2O formed in the cool flame is oxidized by OH in the downstream due to the increased flame temperature. Therefore, an increase of pressure changes the structure of the lean cool flames.

Figure 2(c) compares the dependence of the normalized flame speeds of lean ($\phi = 0.2$) cool flames on the ignition Damköhler number at $P = 1$ and 20 atm, respectively, at $T_0 = 650$ K. The flame speeds are normalized by their speeds $S_{L,Da_{ig}=0}$ at a very low Damköhler number, where the upstream autoignition has negligible impact on flame speed. Figure 2(c) shows that the normalized flame speed increases nonlinearly with the increase of the ignition Damköhler number. Specifically, when Da_{ig} is low (e.g., $Da_{ig} < 0.5$), the effect of ignition acceleration is negligible (usually within 1%) due to the strong temperature-dependent Arrhenius effect. While for $Da_{ig} > 0.5$, the flame speed is exponentially increased. At a low Damköhler number (Fig. 2(a) and (b)), the flame structure agrees well with the classical laminar flame theory where the reactions mainly happen in a narrow reaction–diffusion reaction zone. Nevertheless, it is interesting to note in Fig. 2(c) that for the lean cool flames, the normalized flame speed dependences on the autoignition Damköhler number for pressures at 1 and 20 atm are almost the same although the absolute flame speeds have changed about five times. This close correlation indicates that based on the current kinetic model, the autoignition chemistry for lean cool flames at low and high pressure have similar dependence on local temperature and intermediate species. Of course, the accuracy of the pressure-dependence of the kinetic model needs to be addressed in future studies.

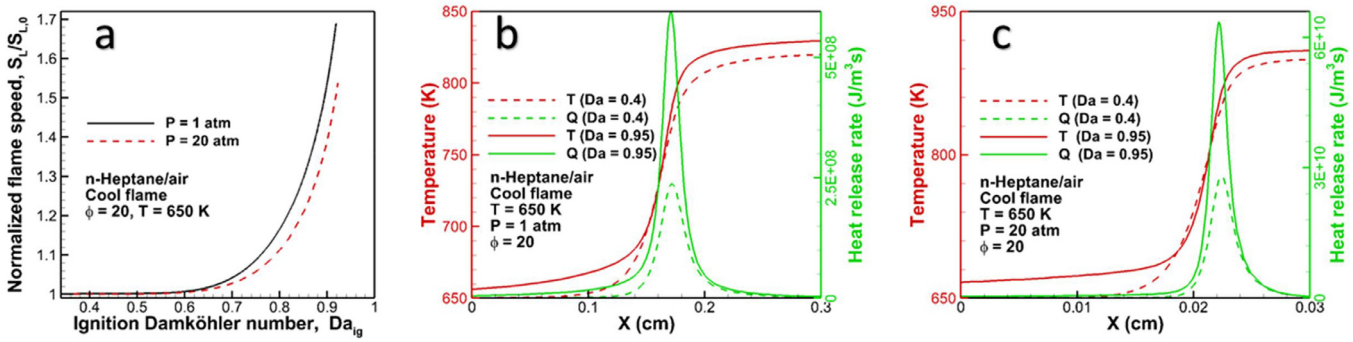

Fig. 3. (a) The relation between the normalized premixed cool flame speed and the ignition Damköhler number for rich cool flames at low and high pressures, T_0 = 650 K, ϕ = 20, P = 1 (Case D) and 20 (Case E) atm. (b) and (c) the rich (ϕ = 20) cool flame structures at T_0 = 650 K, Da_{ig} = 0.4 and 0.95, P = 1 (Case D) and 20 (Case E) atm, respectively.

To illustrate the change of the flame structure with the increase of ignition Damköhler number, Fig. 2(d) shows the comparison of lean cool flame structures, respectively, at Da_{ig} = 0.4 and 0.97 at T_0 = 650 K, P = 1 atm, and ϕ = 0.2. The stream-wise coordinate is shifted to make flame fronts at the low and high ignition Damköhler number conditions locate at the same place for better comparison. It shows clearly that at Da_{ig} = 0.97, although the final peak flame temperature is nearly the same as that of Da_{ig} = 0.4, there is a significant temperature rise and heat release in the convection–diffusion zone. The chemical heat release in the convection–diffusion region is caused by autoignition which raises the initial temperature and changes the mixture composition entering the trailing thin reaction–diffusion zone. Figure 2(e) and (f) shows the comparisons of the volumetric chemical heat release rate and heat conduction rate for a low (Da_{ig} = 0.4) and high (Da_{ig} = 0.97) ignition Damköhler number at T_0 = 650 K, P = 1 atm, and ϕ = 0.2. At the low ignition Damköhler number of Da_{ig} = 0.4, the chemical heat release rate and the heat conduction rate are of the same magnitude, which confirms that at low ignition Damköhler numbers cool flames are governed by the reaction-diffusion process. While at the high ignition Damköhler number of Da_{ig} = 0.97, due to auto-ignition, the chemical heat release in the downstream reaction–diffusion zone is so small compared to that in the upstream auto-ignition reaction region. As such, the diffusive heat transfer rate becomes almost negligible compared with the chemical heat release rate. The lack of the balances between chemical heat release rate and heat conduction rate indicates that the cool flame propagation mode is fundamentally governed by the auto-ignition wave instead of the flame wave. As a result, as shown in Fig. 2(c), the flame speed increases dramatically with the increase of Da_{ig}.

Figure 3 shows, respectively, the cool flame speed dependence on the ignition Damköhler number and the comparison of flame structures at low (Da_{ig} = 0.4) and high (Da_{ig} = 0.95) ignition Damköhler numbers at T_0 = 650 K, P = 1 and 20 atm, respectively, for fuel rich mixture (ϕ = 20). The computed cool flame speeds at ϕ = 20 at 1 and 20 atm are, respectively, $S_{L,Da_{ig}=0}$ = 22.44 cm/s and 7.74 cm/s. It is seen that different from the lean cool flames, the flame speed dependence on the ignition Damköhler number for rich cool flame is affected by the pressure. With the increase of pressure, the increase of the normalized rich cool flame speed is delayed, indicating a higher activation energy for autoignition at a higher pressure. The effect of the pressure increase on flame structure at different ignition Damköhler numbers can be also seen in Fig. 3(b) and (c). Similar to the lean cool flame, with the increase of the ignition Damköhler number, there are both temperature increase and autoignition heat release in the broad pre-flame convection–diffusion zone. However, at P = 20 atm, the heat release rate increases much slower than that of P = 1 atm at the same temperature. More precisely, at Da_{ig} = 0.95, the temperature is 688 K at the 10% of the maximum heat release rate at P = 1 atm. However, at P = 20 atm, the temperature increases to 720 K at the 10% of the maximum heat release rate. It is well-known that the temperature sensitivity of the reaction heat release rate shown in Fig. 3(b) and (c) at a large ignition Damköhler number is mainly governed by the autoignition activation energy. As such, the delayed increase of the normalized cool flame speed at higher pressure shown in Fig. 3(a) suggests that the autoignition activation energy at high pressure is increased at fuel rich conditions, which is different from that of lean cool flames.

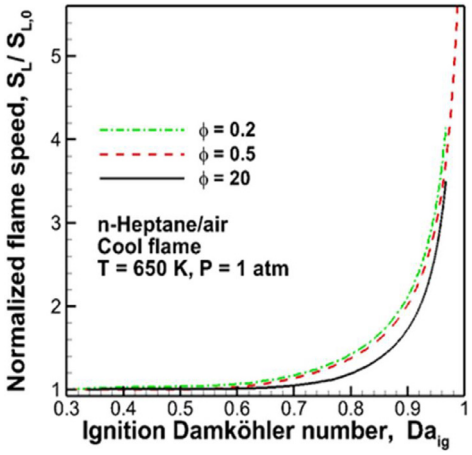

Fig. 4. The relation between the normalized cool flame speed and the ignition Damköhler number at atmospheric pressure for lean and rich cool flames, T_0 = 650 K, P = 1 atm, ϕ = 0.2 (Case A), 0.5 (Case F) and 20 (Case D).

Figure 4 compares the dependence of flame speed on the ignition Damköhler number for lean and rich cool flames at atmospheric pressure, T_0 = 650 K, and P = 1 atm for ϕ = 0.2, 0.5 and 20. First, it is seen that cool flame speeds at all three mixture conditions almost do not change for Da_{ig} < 0.5. When Da_{ig} > 0.5, the flame speeds increase exponentially with the ignition Damköhler number. Secondly, for lean cool flames at ϕ = 0.2 and 0.5, the normalized flame speed dependence on the ignition Damköhler number is very similar. However, the increase of the normalized flame speed with the ignition Damköhler number is delayed for rich cool flames. The results in Figs. 3(a) and 4 suggest that the correlation between the normalized flame speed and the ignition Damköhler number is affected by pressure and mixture equivalence ratio. As will be discussed later, the change of flame

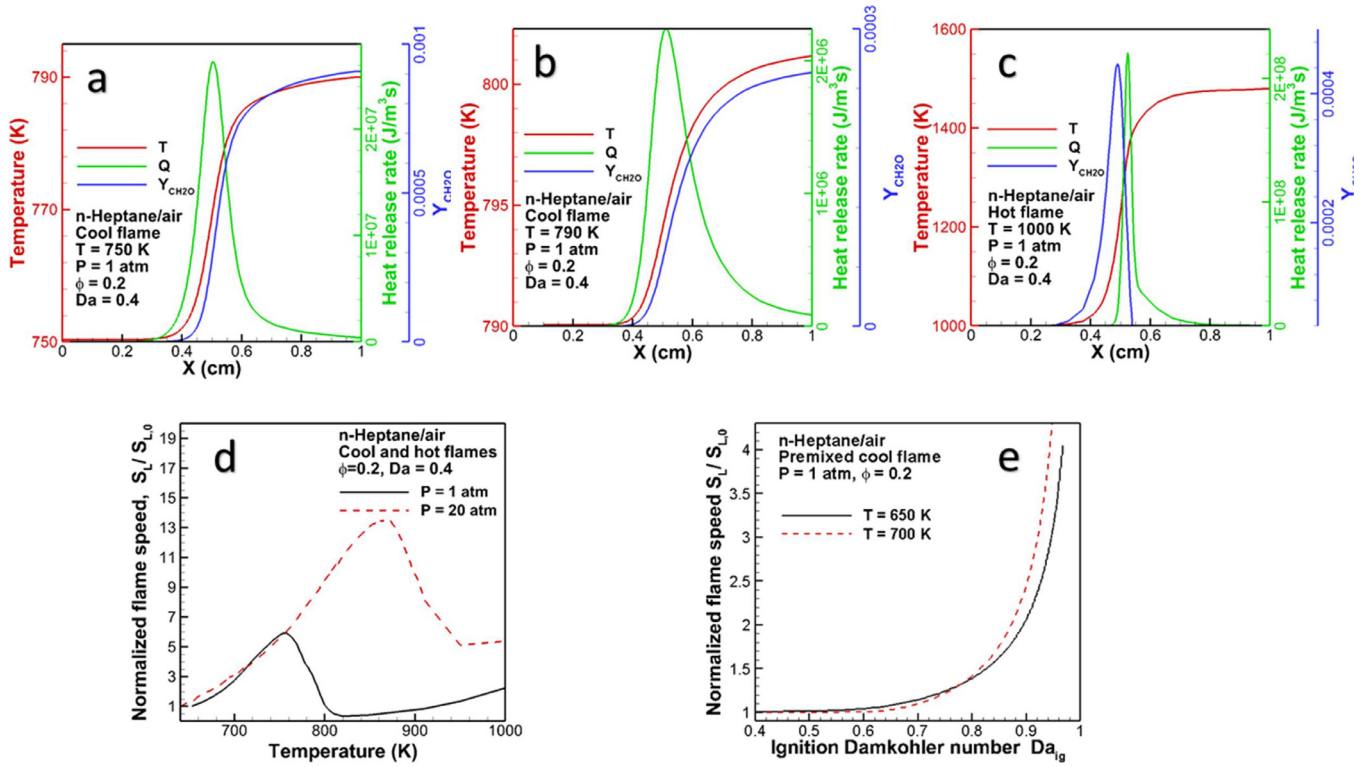

Fig. 5. (a) and (b) the lean ($\phi = 0.2$) cool flame structures at $Da_{ig} = 0.4$, $P = 1$ atm, $T_0 = 750$, 790 K respectively. (c) The lean ($\phi = 0.2$) hot flame structures at $T_0 = 1000$ K, $Da_{ig} = 0.4$, $P = 1$ atm. (d) The relation between the normalized premixed cool flame speed and the initial temperature for lean ($\phi = 0.2$) cool and hot flames at low (1 atm) and high (20 atm) pressures, $T_0 = 650$–1000 K, $P = 1$ and 20 atm, $\phi = 0.2$. (e) The relation between the normalized cool flame speed and the ignition Damköhler number at atmospheric pressure for lean cool flames at different initial temperatures, $T_0 = 650$ and 700 K, $P = 1$ atm, $\phi = 0.2$ (Case A).

speed dependence on ignition Damköhler number is caused by the change of autoignition activation energy.

3.2. Impact of initial temperature and NTC effect on near-limit cool and hot flame flames

It is well-known that both cool and hot flame speeds are strongly affected by temperature. However, it is not clear whether a cool flame can propagate faster than a hot flame at elevated temperature. To answer this question, Fig. 5(a)–(c) shows the structures of cool and hot flames at different initial temperatures, $T_0 = 750$, 790 and 1000 K, for $Da_{ig} = 0.4$, $P = 1$ atm, and $\phi = 0.2$. Figure 5(d) shows the dependence of the normalized flame speed on the initial mixture temperature, for $P = 1$ and 20 atm, respectively. It is seen from Fig. 5(d) that the three initial temperatures at 750, 790 and 1000 K, represent, respectively, the cool flame outside NTC region, the cool flame in NTC region, and the hot flame. At $T = 750$ K, the cool flame structure in Fig. 5(a) shows the flame front temperature is about 770 K after which a large amount of CH_2O is formed. The flame temperature only rise by 40 K and the peak heat release rate is about 2.6×10^7 J/m^{3}s. Comparing to Fig. 2(a), one can conclude that with the increase of initial mixture temperature, the cool flame temperature rise decreases. For a cool flame in the NTC region ($T_0 = 790$ K), Fig. 5(b) shows that with a further increase of the initial temperature, the cool flame temperature rise decreases to only 11 K and the peak heat release rate is reduced to 2.2×10^6 J/m^{3}s. This is mainly due to the NTC effect [42]. In the NTC region, the reactivity of the low-temperature chemistry is inhibited by the acceleration of the decomposition reactions of fuel peroxy radicals ($RO_2 = R + O_2$), hydroperoxyalkyl radicals (QOOH = QO + OH) and peroxy hydroperoxylalkyl radicals (O_2QOOH = QOOH + O_2). The decrease of the RO_2 and QOOH radical pool by these decomposition reactions slows down the overall low-temperature chain-branching pathways [23]. As a result, the flame speed in the NTC region drops significantly (Fig. 5(d)). With the initial temperature further increases to $T = 1000$ K, the role of low temperature chemistry in heat release rate is negligible and the flame chemistry is governed by the high temperature chemistry ($H + O_2 = O + OH$). Figure 5(c) shows that the flame temperature rise increases to 450 K. However, the flame speed remains low due to the large activation energy of the high temperature chemistry.

Figure 5(d) shows the dependence of the normalized flame speed on the initial mixture temperature at $\phi = 0.2$, $Da_{ig} = 0.4$, $P = 1$ and 20 atm, respectively. It is seen that at both low and high pressures, the flame speeds have a non-monotonic dependence on the initial temperature due to the NTC effect. At low temperature, the cool flame speed increases with temperature. In the NTC region, the cool flame speed decreases with the increase of temperature. In the high temperature region, the cool flame becomes a hot flame and the flame speed increases with the initial temperature again. However, it is interesting to notice that the hot flame speeds at such fuel lean conditions are very low. As a result, the peak cool flame speed before the NTC region is much higher than the hot flame. Another interesting observation comes from the comparison between the flame speeds at low and high pressure conditions. Figure 5(d) clearly shows that the peak normalized flame speed at high pressure is much higher than that at low pressure. This is the consequence of the fact that the increase of pressure moves the turnover temperature of NTC to become higher, which enables the autoignition assisted cool flame to have a wider initial temperature range to accelerate. Figure 5(e) shows the relation between the normalized cool flame speed and the ignition Damköhler number at atmospheric pressure for lean cool flames at different initial temperatures, $T_0 = 650$ and 700 K,

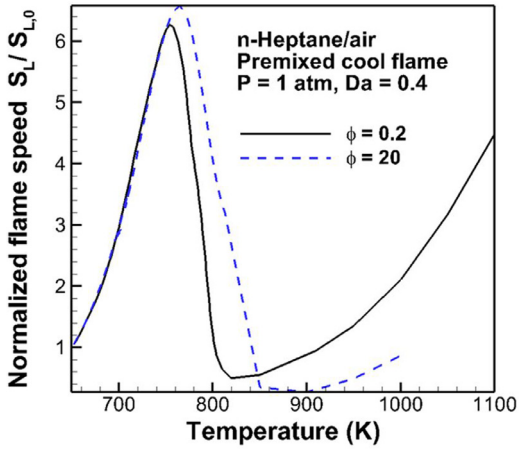

Fig. 6. The relation between the normalized premixed cool flame speed and the initial mixture temperature for lean and rich cool and hot flames at atmospheric pressure, $P = 1$ atm, $\phi = 0.2$ and 20.

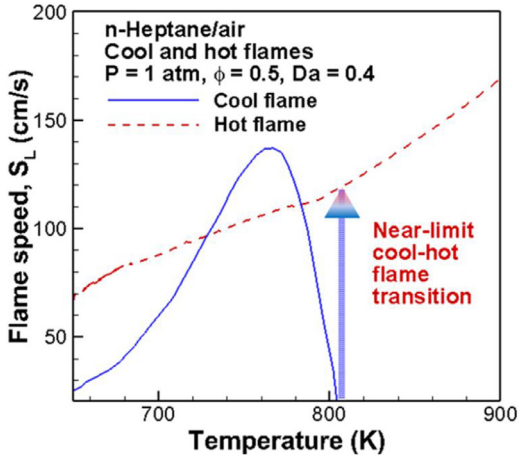

Fig. 7. The relation between the premixed flame speed and the initial temperature for lean cool and hot flames at atmospheric pressure, $P = 1$ atm, $\phi = 0.5$. Note that the mixture equivalence ratio here is within the hot flame lean flammability limit.

$P = 1$ atm, $\phi = 0.2$ (Case A). As can be seen from Fig. 5(e), under a higher initial temperature $T_0 = 700$ K condition, the flame speed of autoignition assisted cool flame increases slightly slower at lower ignition Damköhler numbers ($0.4 < \mathrm{Da_{ig}} < 0.75$), but much faster than that of the $T_0 = 650$ K case at higher ignition Damköhler numbers ($\mathrm{Da_{ig}} > 0.75$). This difference is mainly caused by the negative temperature coefficient effect, i.e., a slower fuel reactivity and a higher global activation energy at a higher temperature after auto-ignition.

Figure 6 shows the comparison of the relations between the normalized flame speed and the initial temperature for lean ($\phi = 0.2$) and rich ($\phi = 20$) cool flames at $P = 1$ atm and $\mathrm{Da_{ig}} = 0.4$. Once again, both lean and rich cool flames have non-monotonic flame speed dependence on the initial mixture temperature due to the NTC effect. Note that the normalized flame speed dependences on temperature for lean and rich mixtures have almost the same correlation before the NTC region. The main difference is that for the rich mixture, the NTC turnover temperature is shifted to a higher temperature by 10 K and results in a higher maximum normalized cool flame speed and a delayed transition from cool flame to hot flame.

For a mixture above the hot flame flammability limit, both a hot flame and a cool flame can exist (Fig. 1). Figure 7 shows the relation between flame speed and the initial mixture temperature for $\phi = 0.5$ at $P = 1$ atm and $\mathrm{Da_{ig}} = 0.4$. Figure 7 clearly shows that both cool and hot flames exist and have different flame speeds under the same condition. For the cool flame, the flame speed changes with the initial temperature non-monotonically due to the NTC effect. However, unlike the sub-limit lean cool flames in Fig. 6, at the end of the NTC region, a further increase of initial temperature will result in an unsteady transition from a cool flame to a hot flame. On the other side, for the hot flame, the flame speed increases monotonically with the increase of the initial mixture temperature. This is because the hot flame does not have an NTC chemistry. Furthermore, as can be seen in Fig. 7, the near-limit cool flame speed is comparable to, or even higher than the hot flame speed over a certain range of temperature. Figure 7 reveals that in near-limit flame speed measurements, care is needed to understand whether the flame is a cool flame or a hot flame so that the kinetic mechanism can be appropriately validated.

3.3. Ignition assisted warm flames and warm flame to hot flame transition

As shown in Fig. 1, a warm flame exists at high pressure below the lean flammability limit of the hot flame. Figure 8(a) shows the warm flame structure at $T_0 = 650$ K, $P = 20$ atm, $\phi = 0.25$. As can be seen in Fig. 8(a), the warm flame has two separated heat release peaks, or in other words, two separated flame fronts: a leading cool flame front and an intermediate temperature flame front. The leading cool flame front temperature is around 720 K and the intermediate temperature flame front temperature is around 930 K, which is above the temperatures for low-temperature chemistry and below those for high temperature chemistry [23]. CH_2O and H_2O_2 are produced in the cool flame and consumed before and in the intermediate temperature flame.

Figure 8(b) shows the relation between normalized flame speed and the ignition Damköhler number for the lean cool ($\phi = 0.2$) and warm ($\phi = 0.25$) flames at $T_0 = 650$ K and $P = 20$ atm. At low ignition Damköhler number ($0.4 < \mathrm{Da_{ig}} < 0.8$), the warm flame speed is largely governed by the speed of the leading cool flame and the cool and warm flames have almost the same response to the increased ignition Damköhler number. However, at high ignition Damköhler numbers, the increase of the warm flame speed starts to slowdown compared with the cool flame.

To better understand the warm flame at large ignition Damköhler numbers, Fig. 9(a) shows the warm flame structures at $P = 20$ atm, $T_0 = 650$ K, $\phi = 0.25$, $\mathrm{Da_{ig}} = 0.4$ and 0.96, respectively. The downstream domain size is extended for the high ignition Damköhler number case ($\mathrm{Da_{ig}} = 0.96$) to show the full flame structures. Figure 9(b) zooms in the leading cool flame front for better observation. The cool flame front location is fixed at the same position for both low and high ignition Damköhler number flames. Figure 9(a) shows that with an increase of ignition Damköhler number, the intermediate temperature flame front moves downstream and is further decoupled from the leading cool flame due to the increase of the leading cool flame speed. As can be seen in Fig. 9(b), the autoignition heat release in the convection and diffusion zone at $\mathrm{Da_{ig}} = 0.96$ is increased. However, the distance between the leading cool flame front and the intermediate temperature flame front becomes much larger from $\mathrm{Da_{ig}} = 0.4$ to 0.96, resulting in a smaller temperature gradient distribution and a weaker diffusive heat transfer from the intermediate flame to the cool flame. This decoupling between the cool and the intermediate flames attributes to a slower increase of warm flame speed with the ignition Damköhler number.

To understand the transition from a warm flame to a hot flame with the increase of the initial mixture temperature, Fig. 10(a) shows the relation between the warm flame speed and the initial mixture temperature at $P = 20$ atm and $\phi = 0.25$. Similar to the

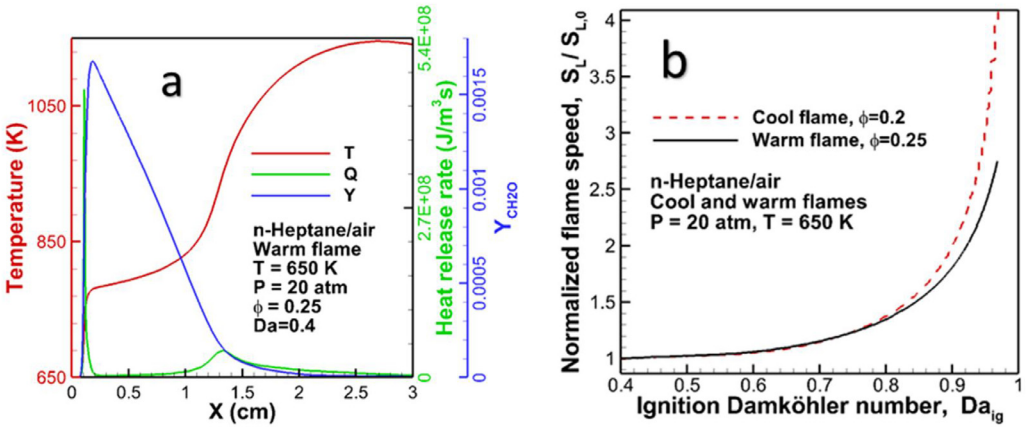

Fig. 8. (a) The warm flame structure at $T_0 = 650$ K, $P = 20$ atm, $\phi = 0.25$, $Da_{ig} = 0.4$. (b) The relation between normalized flame speeds and the ignition Damköhler number for lean cool ($\phi = 0.2$) and lean warm ($\phi = 0.25$) flames at $T_0 = 650$ K, $P = 20$ atm.

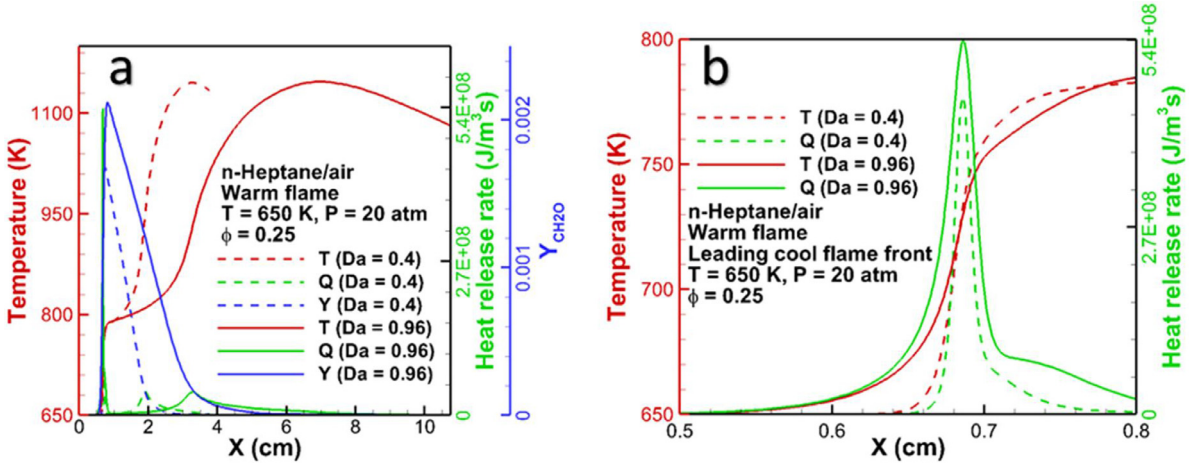

Fig. 9. (a) The warm flame structure at $T_0 = 650$ K, $P = 20$ atm, $\phi = 0.25$, $Da_{ig} = 0.4$ and 0.96. (b) zooms in the leading cool flame structure of the warm flame.

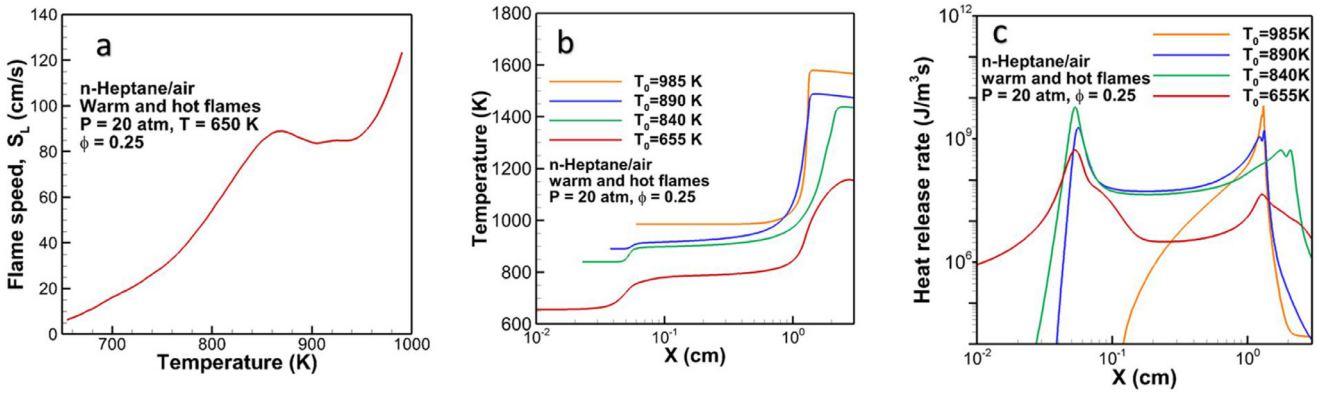

Fig. 10. (a) The relation between flame speed and the initial temperature for warm flames ($\phi = 0.25$) at $T_0 = 650$ K, $P = 20$ atm. (b) and (c) The warm flame temperature and heat release rate distributions at $P = 20$ atm, $\phi = 0.25$, $T_0 = 655$ K (red lines), 840 K (green lines), 890 K (blue lines), 985 K(orange lines), respectively. (For interpretation of the references to color in this figure legend, the reader is referred to the web version of this article.)

cool flame, the warm flame also has a non-monotonic dependence of flame speed on the initial temperature due to the existence of the leading cool flame in the warm flame structure. However, the NTC effect of the warm flame is significantly weaker than that of a cool flame (Figs. 5 and 6). Figure 10(a) shows that in the NTC region starting at $T_0 = 875$ K, the flame speed only decreases slightly from 90.2 cm/s to 80.0 cm/s. At the end of the NTC region (about 960 K), the warm flame transitions to a hot flame and the flame speed increases with temperature rapidly.

To further investigate the warm flame to hot flame transition processes, the distributions of temperature and heat release rate of warm flames at different initial mixture temperatures are shown in Fig. 10(b) and (c), respectively. In both Fig. 10(b) and (c), the intermediate temperature flame fronts are shifted to the same position for better comparison and the upstream domain length is varied since the ignition Damköhler number is fixed. For the initial temperature of $T_0 = 655$ K, there are clearly two heat release rate peaks, which is a typical warm flame structure. As the ini-

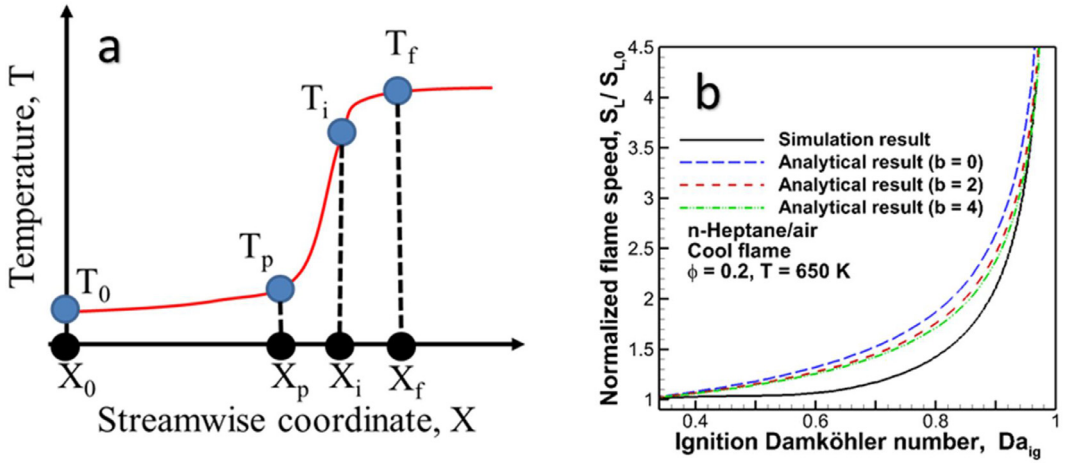

Fig. 11. (a) Illustration of flame structure for the theoretical model of autoignition assisted flame. (b) The comparison for the simulation result and theoretical analysis result for the autoignition assisted lean cool flame at $T_0 = 650$ K, $P = 1$ atm, $\phi = 0.2$, $S_{L,Da_{ig}=0} = 27.2$ cm/s and $T_a = 1871$ K.

tial temperature rises to $T = 840$ K, the heat release rate increases at the cool flame front and the flame speed increases. At the same time, the double-peak heat release rate structure transitions into a triple-peak heat release rate structure contributed respectively by three temperature dependent chain-branching reactions [23]. The third peak near 1400 K is caused by the high temperature chemistry. At this condition, the heat release rate of the cool flame front is still dominant. As the initial temperature rises to $T_0 = 890$ K (inside the NTC region), the low temperature chemistry reactivity is suppressed. At the same time, both the intermediate temperature and high temperature heat releases become stronger. In addition, it is seen that the peak high temperature heat release rate is already larger than the peak intermediate temperature heat release rate. As the temperature further rises, the intermediate temperature heat release rate decreases, and the high temperature heat release becomes dominant. At $T_0 = 985$ K, the warm flame becomes a hot flame with a single high temperature heat release peak. Therefore, the transition between the warm and hot flame is the competition among the heat release rates at low, intermediate and high temperature reaction zones.

3.4. A simple analytical model for prediction of autoignition assisted flame speed

The simulation results have revealed that cool flame speed is strongly affected by the ignition Damköhler number, pressure, and equivalence ratio. For computational modeling with reduced models, it is necessary to predict the dependence of cool flame speed on the ignition Damköhler number in an analytical form.

The numerical results of flame structures at different ignition Damköhler numbers in Figs. 2, 3 and 5 show that, in the flame zone, the assumption of thin reaction-diffusion zone still holds. This implies that the large activation energy assumption [43] can be still adopted at analyzing autoignition assisted cool flame speed.

A simplified three-zone model is shown schematically in Fig. 11(a). In the convection–autoignition zone $x_0 < x < x_p$, autoignition heat release raises the mixture temperature from the initial temperature, T_0, to preheat temperature, T_p. In the convection–diffusion zone $x_p < x < x_i$, the diffusive heat transfer further raises the temperature of the partially burned mixture from T_p to the autoignition temperature of T_i. In the last diffusion–reaction zone $x_i < x < x_f$, reactants are oxidized, and the temperature rises to peak flame temperature, T_f.

Although autoignition in the convection zone generates different intermediate species, the flame reactivity is still mostly governed by the temperature. Therefore, for the sake of simplicity, we will assume that autoignition only modifies the mixture temperature and that other changes are negligible. Consequently, the focus of the current simple model is only placed on modeling the impact of heat release by the autoignition on the flame speed.

Firstly, we assume the global reaction rate can be represented by a one-step Arrhenius reaction with the activation temperature, T_a. Adopting the assumption of constant thermal dynamic properties, the energy equation based on the flame front coordinate in the convection-autoignition zone can be written into the following form by neglecting the diffusive transport:

$$\frac{DT}{Dt} = u\frac{dT}{dx} = \dot{\omega} = AT^b \exp\left(-\frac{T_a}{T}\right), x_0 < x < x_p \tag{2a}$$

Where $\frac{D}{Dt}$ represents material derivative, A is the reduced prefactor of the reaction rate including the specific heat and density, $T_a = E_a/R$ is the activation temperature, b is a constant. Eq. (2a) can be rewritten in Lagrangian coordinate fixed on a certain mixture parcel:

$$\frac{dT}{dt} = AT^b \exp\left(-\frac{T_a}{T}\right), 0 < t < \tau_p \tag{2b}$$

Where τ_p is the residence time for the mixture flowing through convection-autoignition zone (x_0, x_p). Integrating Eq. (2b) from $T_0|_{t=0}$ to $T_p|_{t=\tau_p}$:

$$\int_{T_0}^{T_p} A^{-1}T^{-b}\exp\left(\frac{T_a}{T}\right)dT = \tau_p \approx \tau_f \tag{3a}$$

Note that due to exponential increase of temperature in the convection-ignition zone, the approximation $\tau_p \approx \tau_f$ holds well and is verified by numerical simulations (see the two validation cases in the supplementary material). Eq. (2b) can be used to approximate the ignition delay time τ_{ig} under a constant pressure:

$$\tau_{ig} \approx \int_{T_0}^{T_i} A^{-1}T^{-b}\exp\left(\frac{T_a}{T}\right)dT \tag{3b}$$

Here T_i is the ignition temperature. By substituting Eqs. (3a) and (3b) into Eq. (1): $Da_{ig}\tau_{ig} = \tau_f$, we can have:

$$Da_{ig}\int_{T_0}^{T_i} A^{-1}T^{-b}\exp\left(\frac{T_a}{T}\right)dT = \int_{T_0}^{T_p} A^{-1}T^{-b}\exp\left(\frac{T_a}{T}\right)dT \tag{4}$$

An explicit solution of the autoignition preheating temperature, T_p, can be estimated directly from Eq. (4) by using a one-step reaction model with any A and T_a. If one chooses $b = 2$ for convenience,

a simple explicit expression is given as:

$$T_p = T_a / ln\left[\left(1 - Da_{ig}\right)e^{T_a/T_0} + Da_{ig}e^{T_a/T_i}\right] \quad (5)$$

In fact, any value of b can be used to integrate Eq. (4) and the impact of different choices of b will be discussed later. Furthermore, using the expression for flame speed from the classical laminar flame theory [44]:

$$S_L = \sqrt{\frac{\lambda}{c_p}\frac{T_f - T_i}{T_i - T_p}\frac{\dot{\omega}}{\rho}} \quad (6)$$

In the limit of large activation energy ($T_i \approx T_f$), we can approximate:

$$\frac{T_i - T_0}{T_i - T_p} \approx \frac{T_f - T_0}{T_f - T_p} \quad (7a)$$

$$Da_{ig}e^{T_a/T_i} \approx Da_{ig}e^{T_a/T_f} \quad (7b)$$

Therefore, the laminar flame speed for autoignition assisted flame becomes,

$$S_{L,\,Da_{ig}} = \sqrt{\frac{\lambda}{c_p}\frac{T_f - T_i}{T_i - T_p}\frac{\dot{\omega}}{\rho}} = \sqrt{\frac{\lambda}{c_p}\frac{\dot{\omega}}{\rho}\frac{T_f - T_i}{T_i - T_0}}\sqrt{\frac{T_i - T_0}{T_i - T_p}} = S_{L,Da_{ig}=0}\sqrt{\frac{T_f - T_0}{T_f - T_p}} \quad (8)$$

As a result, an analytical solution of ignition assisted flame speed can be achieved by combining Eqs. (5) and (8) directly:

$$S_L = f\left(Da_{ig}; b, S_{L,Da_{ig}=0}, T_a\right) \quad (9)$$

Here the right hand side of Eq. (9) is an explicit function of the ignition Damköhler number, Da_{ig}, while $S_{L,Da=0}$ is the laminar flame speed at zero ignition Damköhler number.

For example, for the lean cool flame in Case A at $T_0 = 650$ K, $P = 1$ atm, $\phi = 0.2$, the calculated activation temperature based on the flame speed sensitivity on flame temperature perturbation [45] is $T_a = 1871$ K. Together with the computed cool flame speed at zero ignition Damköhler number, $S_{L,Da_{ig}=0} = 27.2$ cm/s, Eq. (9) provides an analytical flame speed dependence on the autoignition Damköhler number with $b = 2$. In addition, for the case $b = 0$ and $b = 4$, there is no closed-formed expression between the flame speed and the ignition Damköhler number, but Eqs. (4) and (8) can still be solved numerically. Figure 11(b) shows the comparison between the simulated and the analytical results with $b = 0$, 2, and 4 respectively for cool flame of this case. All analytical results show that the normalized cool flame speed increases nonlinearly with the ignition Damköhler number and asymptotically goes to infinity as $Da_{ig} \to 1$ and different values of b only change the shape of S_L–Da_{ig} curves minorly. This implies the simple explicit expression coming from Eqs. (5) and (8) is able to depict the S_L–Da_{ig} relation qualitatively well, which demonstrates clearly the activation energy of autoignition in the convection-ignition zone plays a critical role to determine the acceleration effect of the ignition Damköhler number. This result explains the different dependences of flame speeds on the ignition Damköhler number for lean and rich cool flames and the warm flame shown in Figs. 4 and 8. The discrepancy between the analytical result and numerical result in Fig. 11(b) may be caused by the change of species and activation energy in the detailed kinetic model in the process of autoignition.

4. Conclusions

Autoignition assisted laminar cool and warm flame speeds and structures at different ignition Damköhler numbers under elevated temperatures and pressures have been numerically and theoretically modeled over a broad range of equivalence ratios with detailed chemistry. The results show that the flame speeds of both cool and warm flame increase dramatically with the increase of the ignition Damköhler number. Furthermore, the results show the correlations between the flame speed and autoignition Damköhler number depend on equivalence ratio, pressure, temperature, and flame regimes.

The results also shown that due to the NTC effect, the increase of initial mixture temperature leads to a nonmonotonic change in cool flame speed. At sub- and near-limit conditions, the cool flame speed can be significantly faster than that of the hot flame. Moreover, the increase of initial mixture pressure shifts the NTC turnover temperature to a higher temperature thus a higher normalized cool flame speed can be achieved. Furthermore, for mixtures above the hot flame flammability limit, it is found that both cool and hot flames can coexist. There exist dual flame speeds corresponding, respectively, to the cool and hot flames. The cool flame speed remains a nonmonotonic dependence on the mixture initial temperature, but the hot flame speed only monotonically increases with the mixture temperature. In the NTC region, the cool flame speed can still be higher than that of hot flame. At the end of the NTC region, with a further increase in the initial mixture temperature, the steady state cool flame does not exist and becomes a hot flame via an unsteady transition.

For the warm flames, at low ignition Damköhler numbers, the warm flame speed is governed by the leading cool flame. With the increase of ignition Damköhler number, the increase of warm flame speed is slowed down due to the decoupling between the leading cool flame and trailing intermediate temperature flame. Compared to cool flames, with the increase of initial mixture temperature, the non-monotonic dependence of flame speed on mixture temperature due to the NTC effect is weakened. In the NTC region, with the appearance of an extra high temperature reaction zone, the warm flame has three heat release peaks, respectively, corresponding to the cool, intermediate, and high temperature chain-branching pathways. With a further increase of the mixture temperature, the heat release rate from the cool flame zone decreases while the heat release rate in third high temperature reaction zone increases and merges with the reaction zone of intermediate temperature. As a result, a warm flame transitions to a hot flame.

A simple analytical model for the prediction of autoignition assisted flame propagation speed is developed. The results show that the present model predicts the cool flame speed dependence on the ignition Damköhler numbers qualitatively well in comparison to numerical simulations. The good qualitative agreement reveals that the flame speed dependence on ignition Damköhler number is mainly affected by the autoignition activation energy in the convection autoignition zone.

Acknowledgments

The authors would like to thank the grant support from the Army Research Office with grant numbers W911NF-16-1-0076 and W911NF1920127.

Supplementary materials

Supplementary material associated with this article can be found, in the online version, at doi:10.1016/j.combustflame.2019.09.019.

References

[1] R.H. Thring, Homogeneous-Charge Compression-Ignition (HCCI) Engines, SAE International, 1989.
[2] S.L. Kokjohn, R.M. Hanson, D.A. Splitter, R.D. Reitz, Fuel reactivity controlled compression ignition (RCCI): a pathway to controlled high-efficiency clean combustion, Int. J. Engine Res. 12 (2011) 209–226.

[3] J. Hyvönen, G. Haraldsson, B. Johansson, Operating conditions using spark assisted HCCI combustion during combustion mode transfer to Si in a multi-cylinder VCR-HCCI engine, 2005.
[4] Y. Ju, W. Sun, M.P. Burke, X. Gou, Z. Chen, Multi-timescale modeling of ignition and flame regimes of *n*-heptane-air mixtures near spark assisted homogeneous charge compression ignition conditions, Proc. Combust. Inst. 33 (2011) 1245–1251.
[5] Y. Ju, C.B. Reuter, S.H. Won, Numerical simulations of premixed cool flames of dimethyl ether/oxygen mixtures, Combust. Flame 162 (2015) 3580–3588.
[6] Y. Ju, On the propagation limits and speeds of premixed cool flames at elevated pressures, Combust. Flame 178 (2017) 61–69.
[7] C.B. Reuter, S.H. Won, Y. Ju, Flame structure and ignition limit of partially premixed cool flames in a counterflow burner, Proc. Combust. Inst. 36 (2016) 1513–1522.
[8] P. Zhao, W. Liang, S. Deng, C.K. Law, Initiation and propagation of laminar premixed cool flames, Fuel 166 (2016) 477–487.
[9] J. Pan, H. Wei, G. Shu, Z. Chen, P. Zhao, The role of low temperature chemistry in combustion mode development under elevated pressures, Combust. Flame 174 (2016) 179–193.
[10] A. Krisman, E.R. Hawkes, J.H. Chen, The structure and propagation of laminar flames under autoignitive conditions, Combust. Flame 188 (2018) 399–411.
[11] H.J. Emeléus, CCCXCIV.—The spectra of the phosphorescent flames of carbon disulphide and ether, J. Chem. Soc. 129 (1926) 2948–2951.
[12] J.F. Griffiths, T. Inomata, Oscillatory cool flames in the combustion of diethyl ether, J. Chem. Soc. Faraday Trans. 88 (1992) 3153.
[13] H. Pearlman, Brief communication low-temperature oxidation reactions and cool flames at earth and reduced gravity, Combust. Flame 121 (2000) 390–393.
[14] C.B. Reuter, S.H. Won, Y. Ju, Flame Dynamics and Structures of Partially Premixed Cool Flames, American Institute of Aeronautics and Astronautics, Reston, Virginia, 2016.
[15] S.H. Won, B. Jiang, P. Diévart, C.H. Sohn, Y. Ju, Self-sustaining n -heptane cool diffusion flames activated by ozone, Proc. Combust. Inst. 35 (2015) 881–888.
[16] C.B. Reuter, S.H. Won, Y. Ju, Experimental study of the dynamics and structure of self-sustaining premixed cool flames using a counterflow burner, Combust. Flame 166 (2016) 125–132.
[17] O.R. Yehia, C.B. Reuter, Y. Ju, Low-temperature multistage warm diffusion flames, Combust. Flame 195 (2018) 1–28.
[18] Y. Ju, E. Lin, C.B. Reuter, The effect of radiation on the dynamics of near limit cool flames and hot flames, 55th AIAA Aerospace Sciences Meeting (2017), pp. 1–6.
[19] V. Nayagam, D.L. Dietrich, P.V. Ferkul, M.C. Hicks, F.A. Williams, Can cool flames support quasi-steady alkane droplet burning? Combust. Flame 159 (2012) 3583–3588.
[20] T.I. Farouk, D. Dietrich, F.L. Dryer, Three stage cool flame droplet burning behavior of n-alkane droplets at elevated pressure conditions: hot, warm and cool flame, Proc. Combust. Inst. 37 (2019) 3353–3361.
[21] T.I. Farouk, M.C. Hicks, F.L. Dryer, Multistage oscillatory “cool flame” behavior for isolated alkane droplet combustion in elevated pressure microgravity condition, Proc. Combust. Inst. 35 (2015) 1701–1708.
[22] W.S. Affleck, A. Fish, Knock: flame acceleration or spontaneous ignition? Combust. Flame. 12 (1968) 243–252.
[23] Y. Ju, C.B. Reuter, O.R. Yehia, T.I. Farouk, S.H. Won, Dynamics of cool flames, Prog. Energy Combust. Sci. (2019) in press.
[24] T. Zhang, W. Sun, Y. Ju, Multi-scale modeling of detonation formation with concentration and temperature gradients in n-heptane/air mixtures, Proc. Combust. Inst. 36 (2016) 1539–1547.
[25] T. Zhang, W. Sun, L. Wang, Y. Ju, Effects of low-temperature chemistry and turbulent transport on knocking formation for stratified dimethyl ether/air mixtures, Combust. Flame 200 (2019) 342–353.
[26] A.J. Susa, A.M. Ferris, D.F. Davidson, R.K. Hanson, Flame Speed Measurements of Primary Reference Fuels at Elevated Temperatures in a Shock Tube, American Institute of Aeronautics and Astronautics, Reston, Virginia, 2019.
[27] J.B. Martz, G.A. Lavoie, H.G. Im, R.J. Middleton, A. Babajimopoulos, D.N. Assanis, The propagation of a laminar reaction front during end-gas auto-ignition, Combust. Flame. 159 (2012) 2077–2086.
[28] J.B. Martz, H. Kwak, H.G. Im, G.A. Lavoie, D.N. Assanis, Combustion regime of a reacting front propagating into an auto-igniting mixture, Proc. Combust. Inst. 33 (2011) 3001–3006.
[29] A. Ansari, J. Jayachandran, F.N. Egolfopoulos, Parameters influencing the burning rate of laminar flames propagating into a reacting mixture, Proc. Combust. Inst. 37 (2019) 1513–1520.
[30] W. Zhang, M. Faqih, X. Gou, Z. Chen, Numerical study on the transient evolution of a premixed cool flame, Combust. Flame. 187 (2017) 129–136.
[31] M. Faghih, H. Li, X. Gou, Z. Chen, On laminar premixed flame propagating into autoigniting mixtures under engine-relevant conditions, Proc. Combust. Inst. 37 (2019) 4673–4680.
[32] W. Sun, S.H. Won, X. Gou, Y. Ju, Multi-scale modeling of dynamics and ignition to flame transitions of high pressure stratified n-heptane/toluene mixtures, Proc. Combust. Inst. 35 (2015) 1049–1056.
[33] S. Dooley, F.L. Dryer, T.I. Farouk, Y. Ju, S. Hee Won, Reduced kinetic models for the combustion of jet propulsion fuels, 51st AIAA Aerospace Sciences Meeting, 2013 (2013), pp. 1–7.
[34] W. Sun, Z. Chen, X. Gou, Y. Ju, A path flux analysis method for the reduction of detailed chemical kinetic mechanisms, Combust. Flame 157 (2010) 1298–1307.
[35] R.J. Kee, J.F. Grcar, M.D. Smooke, J.A. Miller, E. Meeks, PREMIX: a Fortran program for modeling steady laminar one-dimensional premixed flames, Sandia National Laboratories Report SAND85-8249, 1985.
[36] Y. Ju, T. Niioka, Combustion theory and modelling computation of NO_x emission of a methane–air diffusion flame in a two-dimensional laminar jet with detailed chemistry computation of NO_x emission of a methane–air diffusion flame in a two-dimensional laminar jet with de, Combust. Theory Model. 13 (1997) 243–258.
[37] Z. Chen, Y. Ju, On the Accurate Determination of Flame Speeds at Normal and Elevated Pressures by Using a Spherical Bomb: The Effects of Compression and Stretch, American Institute of Aeronautics and Astronautics, Reston, Virigina, 2007.
[38] Z. Chen, M.P. Burke, Y. Ju, Effects of lewis number and ignition energy on the determination of laminar flame speed using propagating spherical flames, Proc. Combust. Inst. 32 (2009) 1253–1260.
[39] C.-W. Shu, High-order finite difference and finite volume weno schemes and discontinuous Galerkin methods for CFD, Int. J. Comut. Fluid Dyn. 17 (2003) 107–118.
[40] W. Sun, Y. Ju, A multi-timescale and correlated dynamic adaptive chemistry and transport (CO-DACT) method for computationally efficient modeling of jet fuel combustion with detailed chemistry and transport, Combust. Flame 184 (2017) 297–311.
[41] X. Gou, W. Sun, Z. Chen, Y. Ju, A dynamic multi-timescale method for combustion modeling with detailed and reduced chemical kinetic mechanisms, Combust. Flame 157 (2010) 1111–1121.
[42] F. Battin-Leclerc, Detailed chemical kinetic models for the low-temperature combustion of hydrocarbons with application to gasoline and diesel fuel surrogates, Prog. Energy Combust. Sci. 34 (2008) 440–498.
[43] Y.B. Zeldovich, D.A. Frank-Kamenetskii, On the theory of uniform flame propagation, 1938.
[44] I. Glassman, R. Yetter, Combustion, Elsevier, 2015.
[45] Y.B. Zeldovich, Regime classification of an exothermic reaction with nonuniform initial conditions, Combust. Flame. 39 (1980) 211–214.